Ionosphere–thermosphere coupling

R. Sridharan

Physical Research Laboratory, Ahmedabad 380 009, India

Unlike other topics which discuss the coupling between two different regions that are physically separated, the topic of ionosphere–thermosphere coupling deals with the interactive processes between two different constituents namely, the charged and the neutral particles in the same region. Due to the geomagnetic control of motion of the charged particles, the two different constituents of the upper atmosphere behave as independent parts of a mutually coupled system. Some of the coupling processes and their consequences are presented and discussed.

Our earth's neutral atmosphere has been classified into layers based on its thermal structure. While there is a decrease of temperature with altitude in the troposphere and mesosphere there is an increase of the same in the other two regions namely the stratosphere and thermosphere (Figure 1 *a*). As could be seen in Figure 1 *a*, thermosphere refers to that altitude region between about 90–400 km and spans from the coldest (~170 K) to the hottest (1000–2000 K) regions, thus constituting a steep temperature gradient. At this height diffusive equilibrium prevails in the different atmospheric species and as a consequence the dominant molecular composition at lower heights gives way to a predominantly atomic composition higher above (Figure 1 *b*), significant amount of solar EUV radiation is absorbed in this region and this interaction is primarily responsible for the formation of *E* and *F* regions of the ionosphere (Figure 1 *c*). A variety of physical, chemical and dynamical processes result in the redistribution of ionization such that the maximum of ionization content is retained in the *F* region of the ionosphere. Figure 1 *c* depicts the layered structure of the ionosphere with the typical thermal structure in the background. The charged particle densities are of the order of 1 in 10^6 during daytime conditions. Due to infrequent collisions between the charged particles and the neutrals in these heights, the motion of the charged particles is effectively controlled by the earth's magnetic field lines. Such geomagnetic control adds new dimensions to the interactive processes between the neutrals and ionized part of the upper atmosphere.

Historically, the different regions/layers of the atmosphere, representing the neutral and ionized parts have been studied as independent entities and the mutual coupling between them had been ignored. The reasons for this approach had been numerous and include their differing chemistry and dynamics and also their accessibility to investigation by different experi-

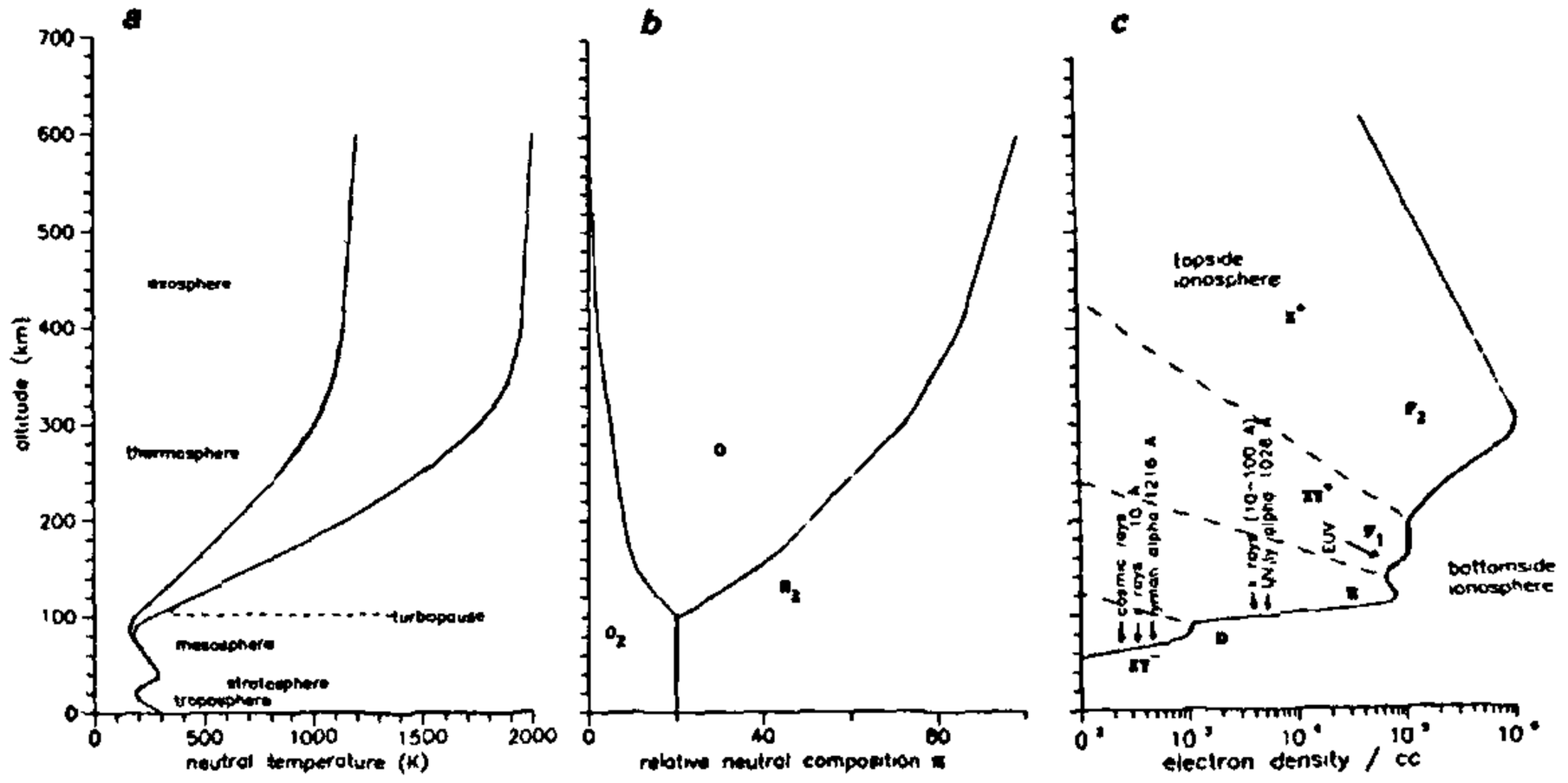

Figure 1. Representative structure of the neutral and ionized parts of the atmosphere. *a*, Thermal structure and the classifications made on its basis. *b*, The relative neutral composition with altitude. Up to the turbopause thorough mixing prevails beyond which the different constituents are in diffusive equilibrium. *c*, Structure of the ionosphere and the agencies that cause such a structure.

mental techniques. For example, the ionosphere could conveniently be probed from ground by means of radio probing methods while studies on neutral atmospheric processes could only be carried out by means of optical techniques.

The dominant heat source of the thermosphere is the ultraviolet and extreme ultraviolet radiation from the sun. The daily variation in the level of solar radiation would induce changes in the winds, temperature, pressure and density fields. Such changes constitute the so-called solar tides. As a consequence of this sort of thermal energy input, what one encounters is a 'hot' dayside and a 'cold' nightside of the earth. Pressure/temperature gradients are set up and energy and momentum are transported in the zonal direction from the hot dayside to the cold nightside. Figure 2*a* depicts the circulation patterns that get set up and, due to the earth's rotation on its own axis it would manifest as a diurnal variation[1]. Apart from this, due to the inclination of the earth's spin axis with its orbital plane around the sun, one encounters a warm summer and a cold winter hemisphere which results in interhemispheric transport in the meridional direction (Figure 2*b*)[1]. In addition to the solar photon flux, the upper atmosphere receives energy from the solar wind through the magnetosphere in the form of precipitation of high energy particles and electric fields. Such interaction processes get enhanced during geomagnetically disturbed periods. At high latitudes, the magnitude of the solar wind/magnetospheric energy influx often dominates the heating from UV and EUV absorption and can be visualized through Figure 2*c*[1]. The first observational evidence for the neutral atmosphere to get heated up during geomagnetic storm was obtained by Jacchia (1959)[2] by monitoring the orbital decay of near earth artificial satellites. Later experiments onboard OGO-VI and ESRO-4 satellites provided the morphology of the disturbed atmosphere[3,4]. These studies demonstrated that there is a gradual increase in the N_2 concentration of the disturbed upper atmosphere from two high latitudes. The latitudinal gradient arises because the solar wind/magnetospheric energy is primarily deposi-

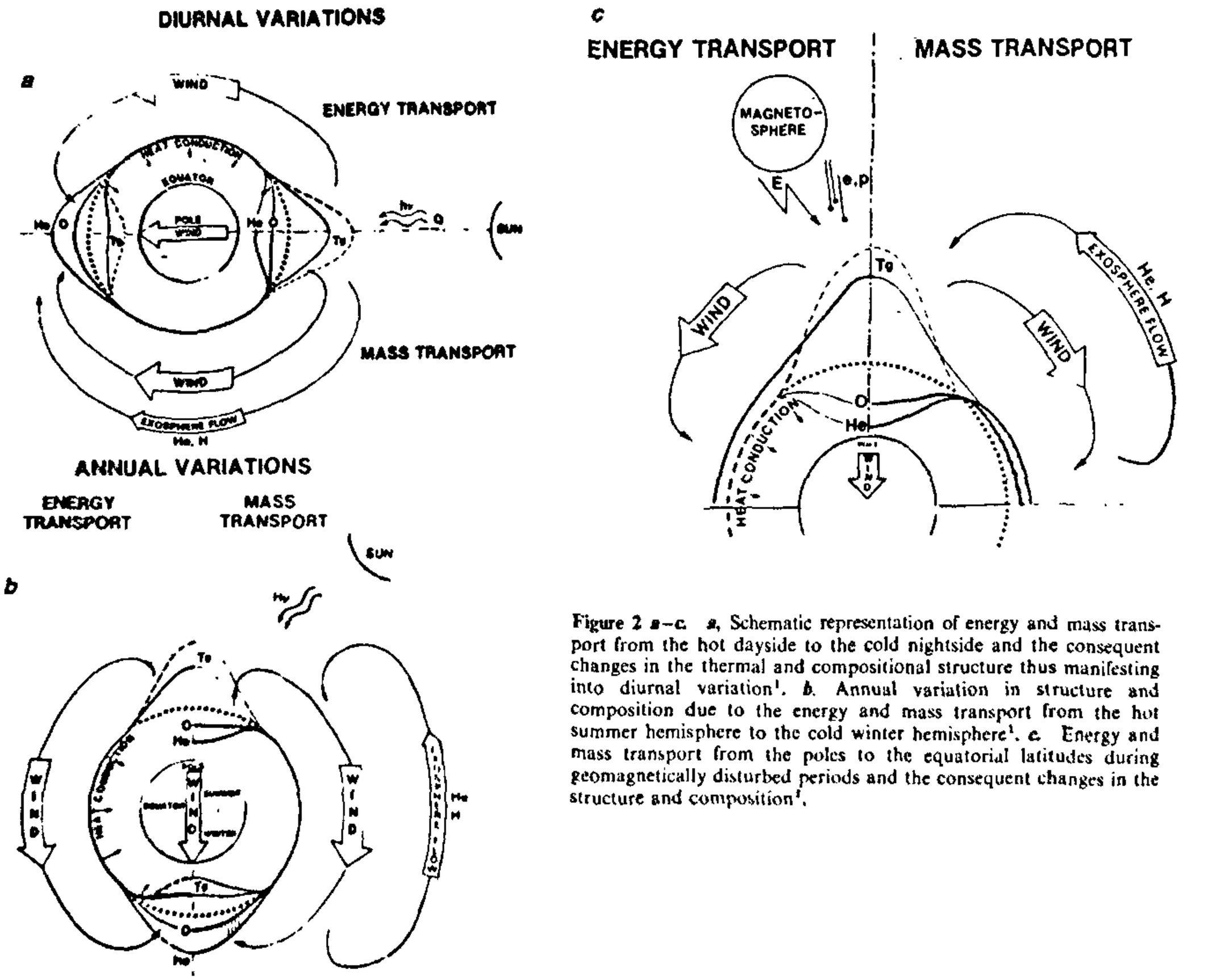

Figure 2 *a–c*. *a*, Schematic representation of energy and mass transport from the hot dayside to the cold nightside and the consequent changes in the thermal and compositional structure thus manifesting into diurnal variation[1]. *b*. Annual variation in structure and composition due to the energy and mass transport from the hot summer hemisphere to the cold winter hemisphere[1]. *c*. Energy and mass transport from the poles to the equatorial latitudes during geomagnetically disturbed periods and the consequent changes in the structure and composition[1].

ted in the auroral *E*-region, causing a vertical upwelling of N_2 in the auroral *F*-region[5]. On occasions significant deposition of energy occurs even at mid-latitudes[6]. Since the storm energy source was generally believed to be restricted only to high latitude auroral regions[7] it was believed that the magnetic activity induced/related changes in the atmospheric/ionospheric parameters over low and equatorial latitudes could only be due to disturbance transport[8]. Mayr and Volland[9] and Hays *et al.*[5] theoretically demonstrated that the cellular upwelling initiated due to the heating in the auroral zone results in lateral flow thus extending the effects of the heating on a global scale. There are several examples which indicate the above picture to be oversimplistic. Experimental evidences have been obtained for direct deposition of energy even in the equatorial zone causing significant changes in the thermal structure and composition (*Figure 3 a, b*)[10,11]. The exact mechanism of deposition of energy is still to be understood.

Over and above the diurnal, seasonal and latitudinal variabilities, one encounters several wave phenomena superposed over the quasi-steady winds and drifts. Their periodicities range from a few minutes to several hours. These waves are either generated *in situ* in the thermosphere or get propagated from lower below. These wavelike perturbations may either be systematic as in tidal forcings or impulsive as it happens during a geomagnetic storm.

Since the charged particles are formed out of the surrounding neutral atmosphere, and as they form an extremely small part of the overall concentration, any change in the fundamental properties of the neutral atmosphere like structure, energetics, composition and dynamics would have its repercussions in the charged particle distribution. However, due to the geomagnetic confinement of the movement of the charged particles they offer considerable resistance to the neutral motion referred to as *Ion drag*. It is now well accepted that the ionospheric magnetoplasma could act as a source or sink of momentum for the neutral thermospheric gas[12].

The neutral gas momentum equation in its simplifed form could be written as[13]:

$$\partial \bar{U}/\partial t = \varepsilon(\bar{V}_i - \bar{U}) + \text{other terms} \qquad (1)$$

where $\bar{U}$ is the neutral wind velocity, t the time and $\bar{V}_i$ the plasma drift velocity. $\varepsilon = \sigma_1 B^2/\rho_0$, where σ_1 is the Pedersen conductivity, B the magnetic field intensity and ρ_0 the neutral mass density.

The plasma drift velocity $\bar{V}_i$ is equal to $(\bar{E} \times \bar{B})/B^2$. At high latitudes $\bar{V}_i$ is quite dominant and acts as a driver for the thermospheric motions. At low latitudes $\bar{E} \times \bar{B}$ drifts are normally smaller in magnitude as compared to the neutral motions ($\bar{U}$). In this case $\bar{V}_i$ would be directed along $\bar{B}$ and is equal in magnitude to the field-aligned component of the thermospheric wind $\bar{U}$ i.e.

$\bar{V}_i \bar{U}_\parallel = u \sin D \cos I + v \cos D \cos I - w \sin I$, where $\bar{U}_\parallel$ is the field-aligned component of $\bar{U}$, u the geographic eastward component of $\bar{U}$, v the geographic northward component of $\bar{U}$, w the vertical component of U; I the magnetic dip and D the magnetic declination.

Neglecting the magnetic declination and the vertical wind effects the momentum equations for the zonal and meridional directions could be written as[13].

$$\partial u/\partial t = -\varepsilon u + \text{other terms}, \qquad (2)$$

$$\partial v/\partial t = -\varepsilon v \sin^2 I + \text{other terms}. \qquad (3)$$

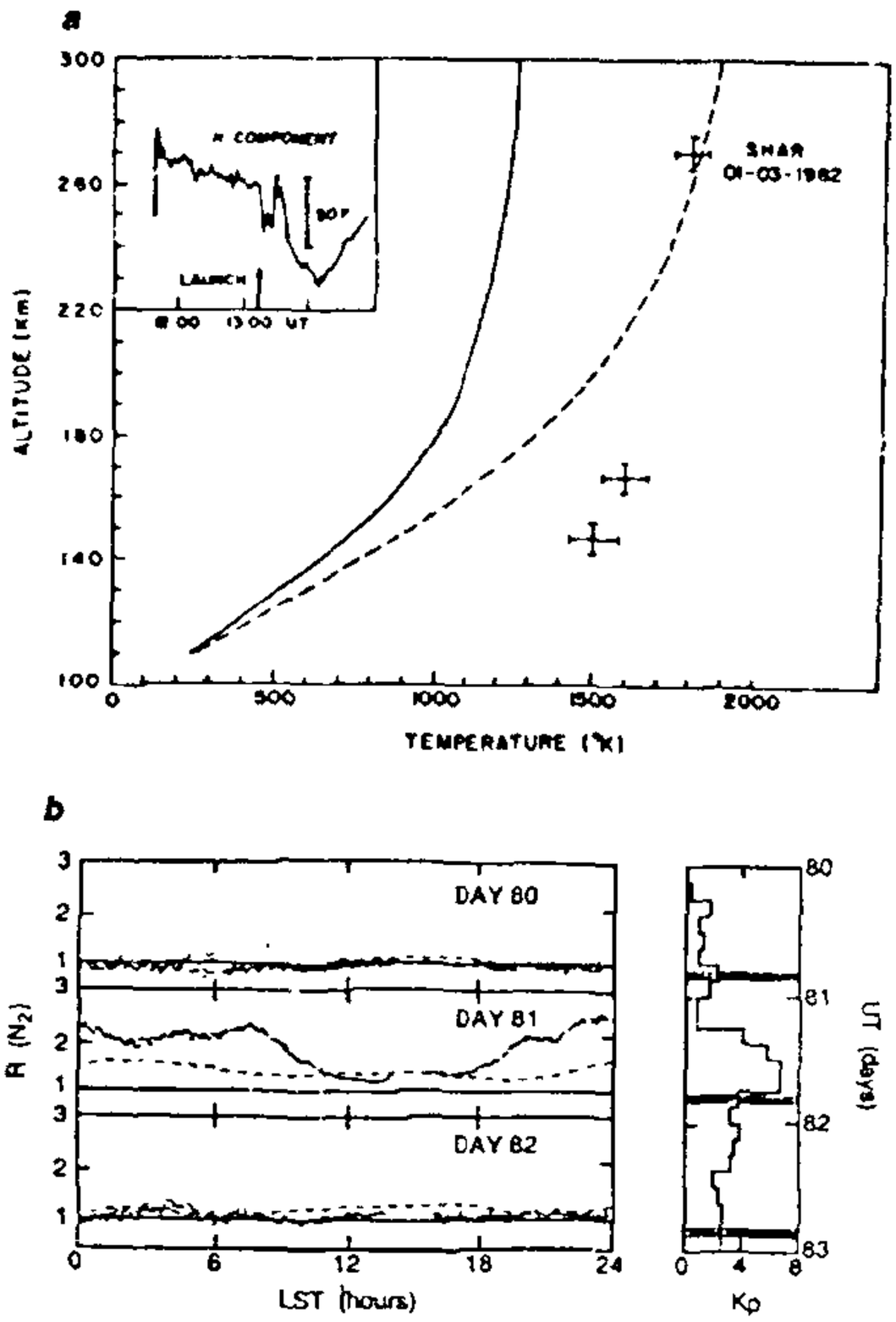

Figure 3 *a, b*, *a*, Evidence by *in situ* measurements of neutral temperature (spectroscopically determined) for the direct deposition of energy at the equatorial latitudes during a geomagnetic storm. The continuous curve represents the model values for this occasion. The dashed curve is the model profile for the measured exospheric temperature. Localized heating effects are seen around 140 km[10]. *b*, Observed N_2 concentration over the equatorial zone (continuous curve) along with the model (dashed curve) as measured by the Atmospheric Explorer AE-E satellite for three orbits made on consecutive days (80–81) in 1979 along with the corresponding K_p values confirming the direct deposition of energy over the equatorial latitudes. The shaded portion represents the duration of the orbit[11].

In both equations (2) and (3) the ionospheric plasma effect appears as a decelerating force, or drag on the neutral wind and hence the term 'ion drag'. It is a frictional force and always opposes the motion. As is evident from the above two equations, the drag is maximum in the zonal direction and is proportional to the zonal wind. In the meridional direction, however, it is maximum at the poles and zero over the equator. As it is dependent on the magnetic dip, there is a latitude dependence of the drag force. The field-aligned component of the meridional wind inturn serves to transport ionization along the field lines and thus modulates the drag offered to the zonal flow. The vertical plasma drift ($v \cos I \sin I$) is maximum at $I = 45°$ for any given wind speed.

With this background some of the interactive processes that exist between the ionosphere and thermosphere would be presented and discussed. Ample evidences exist through systematic coordinated measurements for the close coupling to prevail between the thermosphere and the F-region of the ionosphere.

One of the elegant concepts that describes the coupling between these two constituents of the upper atmosphere is the servo principle by Rishbeth[14,15]. It provides a convenient analytical description of the ionospheric F_2-peak, or the height of the maximum electron density (h_{max}), which is one of the observable parameters. The h_{max} is determined by both the loss of ionization and its replenishment due to transport which in this case is through plasma diffusion. For an atmosphere consisting of a single species and for an F-layer represented by a simple Chapman layer, h_{max} is shown to be located where

$$\beta_m \simeq \frac{k D_m \sin^2 I}{2H^2 (kac - 1)}, \tag{4}$$

where β_m is the effective loss coefficient, D_m the plasma diffusion coefficient (O^+ through O), H the scale height of atomic oxygen O, I the magnetic dip and k, a, c are constants[15].

The balance height h_{max} is referred to as the night stationary level under simple photochemical equilibrium conditions.

The other parameters that would alter h_{max} are the neutral winds in the meridional direction and the electric fields. The effect of these two parameters would be to alter the balance height to a new level. For example, a poleward wind $\bar{U}_p$ would push the F layer down as[16]:

$$\bar{U}_p = (h_0 - h_{max})/\alpha,$$

where $\alpha = 2H^2/D_m(k+1) \sin I$ and h_{max} and h_0 refer to

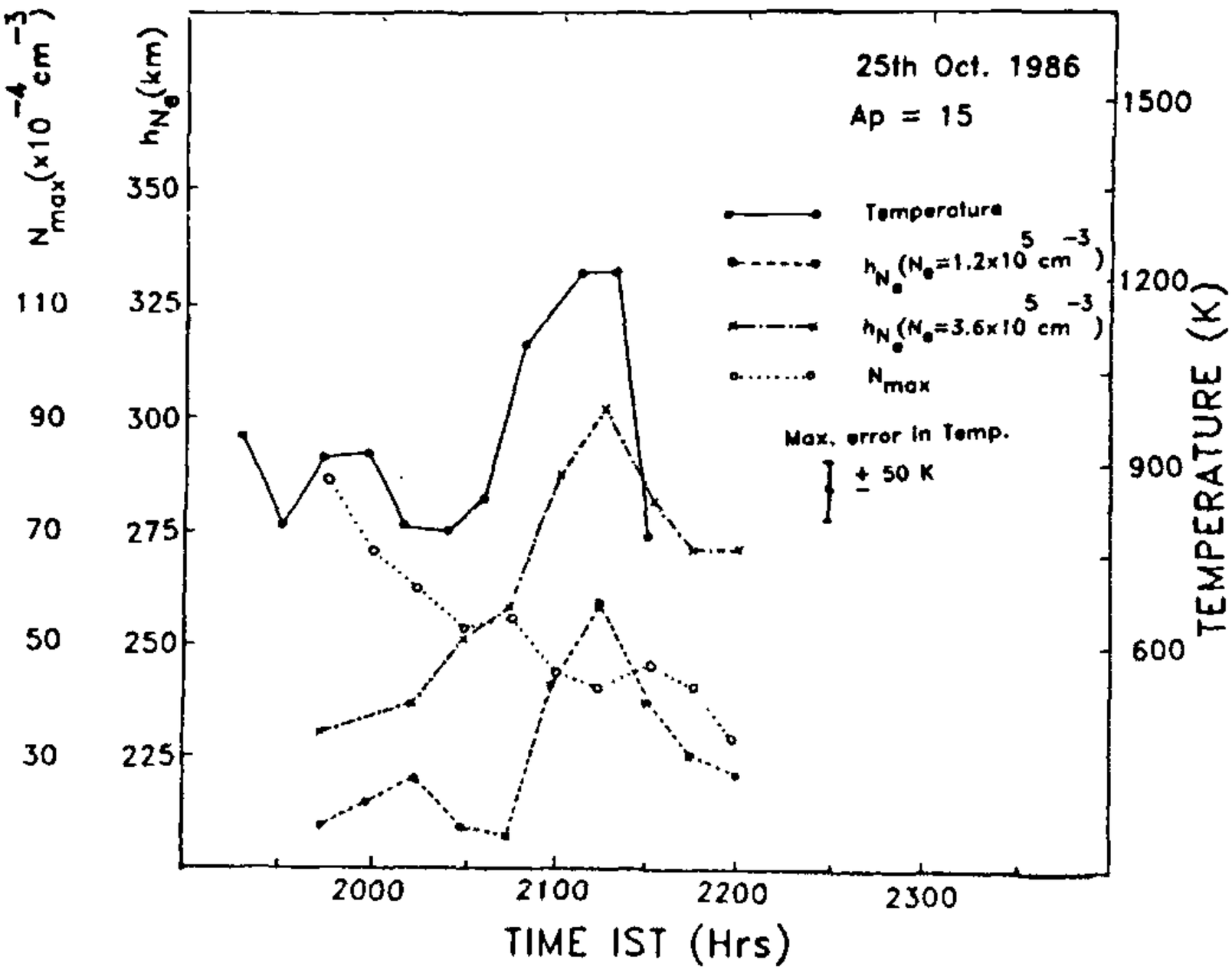

Figure 4. Response of the low latitude (Ahmedabad/Mt. Abu) F-region to the changes in the neutral temperature demonstrating the close coupling between the low latitude thermosphere and ionosphere[17].

the balance heights with and without the winds.

Superposition of an electric field would alter h_{max} still further by[16]

$$U_p = [(h_0 - h_{max})/\alpha] + E/(B \sin I). \quad (5)$$

The servo principle originally proposed for mid-latitude locations has been found to be applicable to low latitudes as well. These conclusions were arrived at by means of coordinated optical and radio sounding measurements from Mt. Abu and Ahmedabad[17] (Figure 4).

The optical probing of the appropriate airglow emissions from the thermosphere is one of the ideal means to investigate the thermosphere–ionosphere coupling. The reasons are as follows—one of the prominent natural airglow emissions from the thermosphere is the OI 630.0 nm line emission originating around 250 km with an emission layer semithickness of ~50 km. During night-time conditions the sequence of chemical reactions that give rise to this emission is:

O^+ the dominant ionic species [$O^+ \sim N_e$] undergoes a charge exchange reaction with O_2

$$O^+ + O_2 \rightarrow O_2^+ + O. \quad (6)$$

The resultant O_2^+ dissociatively recombines with ambient electrons such that

$$O_2^+ + e \longrightarrow O^* + O^*, \quad (7)$$

$$O^* \longrightarrow O + h\nu \text{ (OI 630.0 nm)}. \quad (8)$$

The excited atomic oxygen O^* is in a metastable state having a typical lifetime of ~410 s for OI 630.0 nm emission. During this time interval the excited species would experience sufficient number of collisions so as to attain thermal equilibrium with the ambient species. High resolution emission line profile measurements would yield the dynamical parameters pertaining to the neutral atmosphere. For example, the broadening of the emission line is proportional to the kinetic temperature and the shift in the centre of the emission line is proportional to the line-of-sight velocity of the medium as a whole. While the spectral information yields data on the neutral atmospheric parameters, the intensity of the emission line has been shown to be proportional to the F-region plasma density. Therefore with a single set of measurements one could talk about both the neutral and ionized parts of the upper atmosphere. Radio sounding methods like, for instance, ionospheric sounders give us data on the altitudewise distribution of

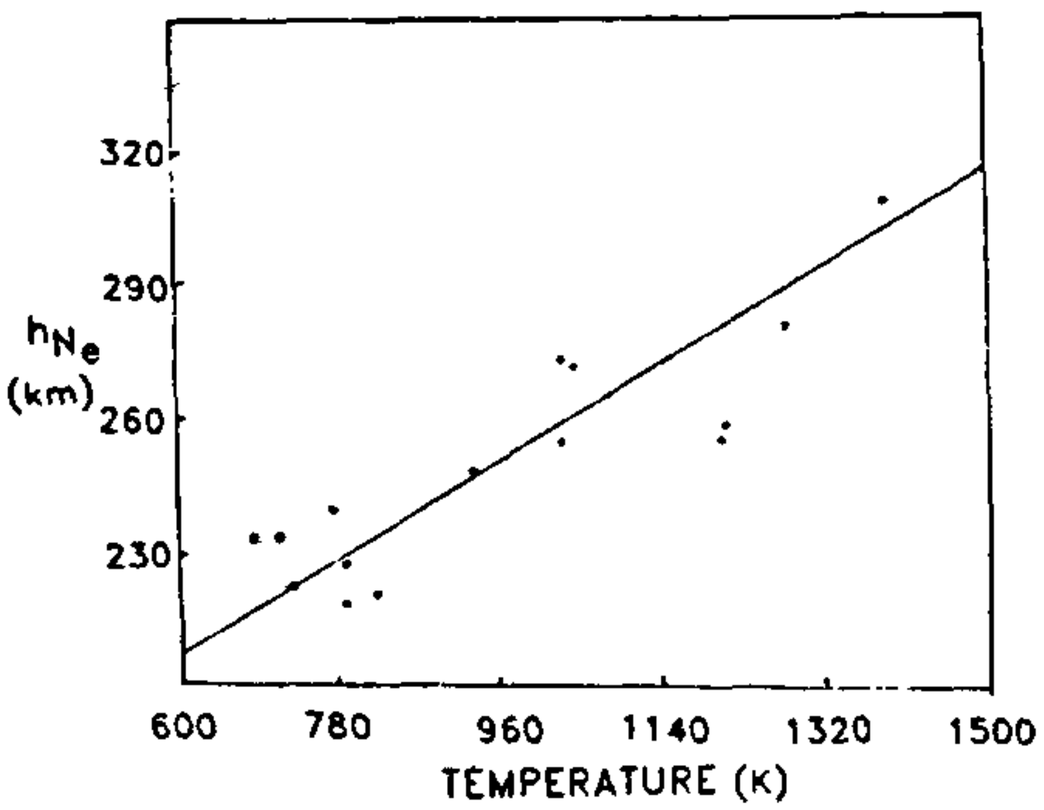

Figure 5. Relation (11 ± 4 km/100 K) of the base height of the F-region to the neutral temperature based on coordinated ionospheric and thermospheric measurements[17].

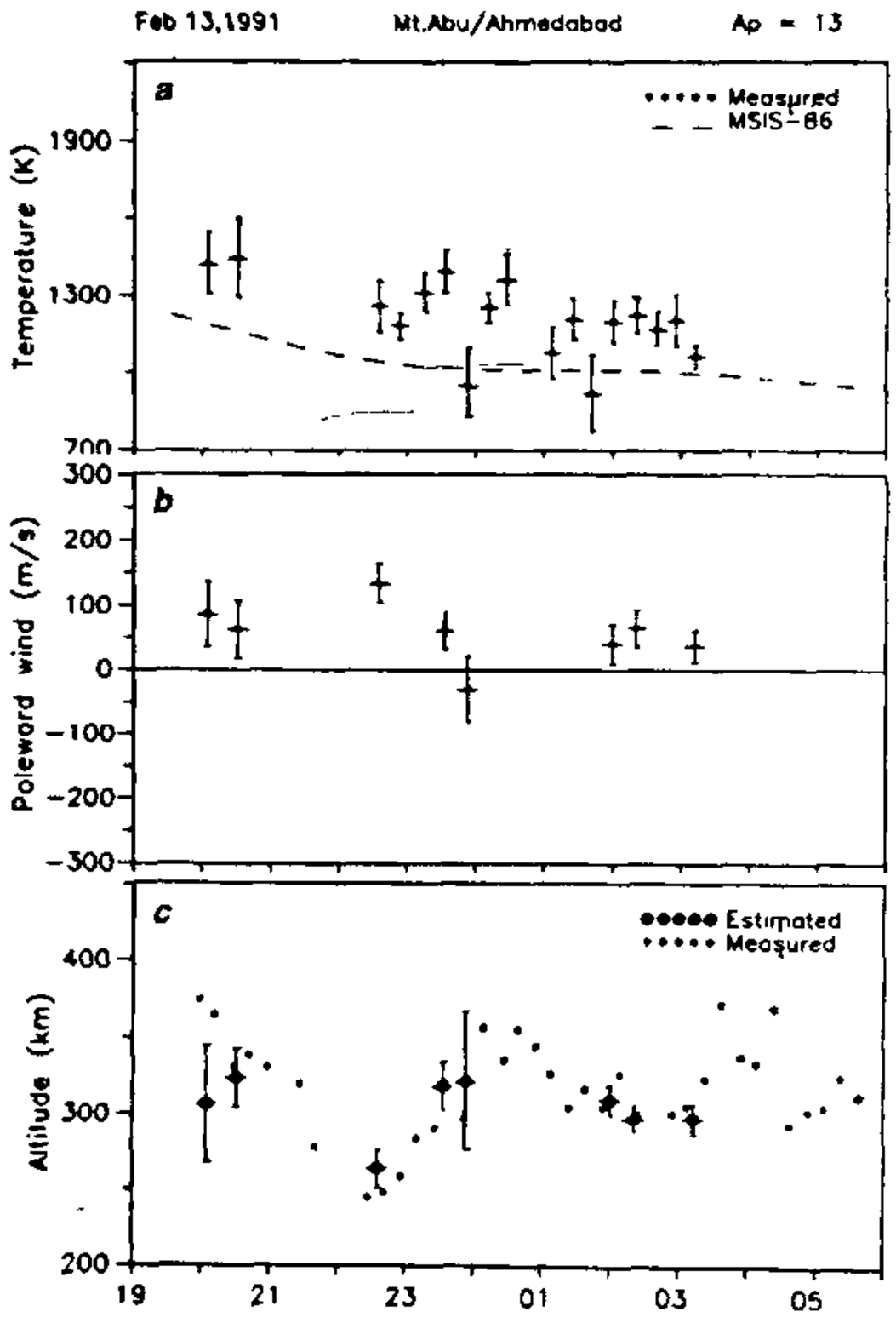

Figure 6. Behaviour of the low latitude thermosphere/ionosphere system. *a*, Measured and model neutral temperature (T_n) over Mt. Abu. *b*. Spectroscopically determined meridional neutral winds (U). *c*. Estimated h_{max} for the measured T_n and U based on the servo principles along with the independently measured h_{max} using ground-based ionospheric sounder. The validity of the servo principles is experimentally demonstrated[18].

the *F*-region plasma density. Coordinated measurements with high resolution Fabry-Perot spectrometers and ionosonde would enable investigation on the thermospheric/ionospheric system and the eventual coupling between them.

Individual case studies have revealed that the neutral temperatures have a one-to-one correspondence with the movement of the *F*-layer yielding 11 ± 4 km/100 K (Figure 5) as is expected in accordance with the servo principles of Rishbeth[15]. As a second step, the measured neutral temperatures were made use of in the servo equations to determine the balance height h_0, and the effect of measured meridional winds is incorporated in arriving at the resultant h_{max}. These estimated h_{max} values were compared with independent h_{max} measurements using ground-based ionosonde. The agreement had been fairly good (Figure 6) despite the electric field effects not being accounted for [18]. In fact the deviations between the estimated and measured h_{max} could be used to derive the third parameter namely, the electric field[18]. Such case studies demonstrate the close coupling that prevails between the neutral and ionized parts of the upper atmosphere.

Though numerous examples for the prevailing close coupling are available from satellite measurements at high latitudes which results in large-scale features, temporal variations and spatial structures, there are many interesting phenomena at low and equatorial latitudes as well.

One of the prominent features of this region is the development of the equatorial ionization anomaly (EIA) and the associated interactive processes. EIA primarily gets formed due to the electrodynamical processes over the equator (Figure 7). With the intensification of the primary east-west electric field from morning to noon, the *F*-region plasma gets lifted up due to the $\bar{E} \times \bar{B}$ effect only to diffuse along the geomagnetic field lines to higher latitudes. This eventually manifests as two crests of ionization on either side of the dip equator with a trough right overhead. Such non-uniform distribution of *F* region plasma would then have its repercussions on the neutral constituents and their behaviour. The

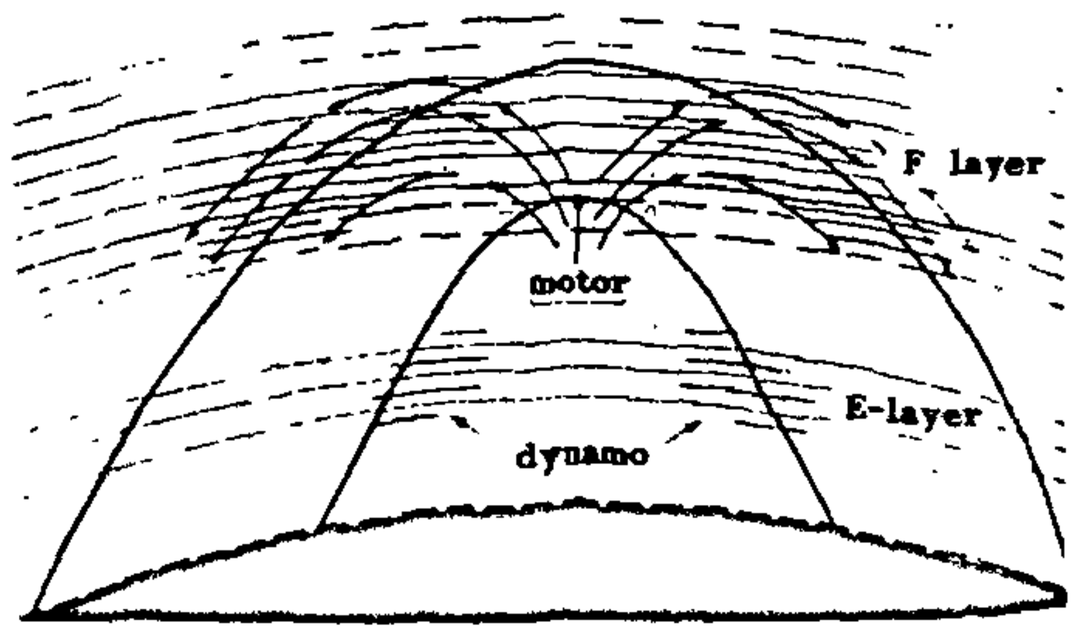

Figure 7. Conceptual diagram depicting the equatorial fountain effect resulting in the generation of EIA.

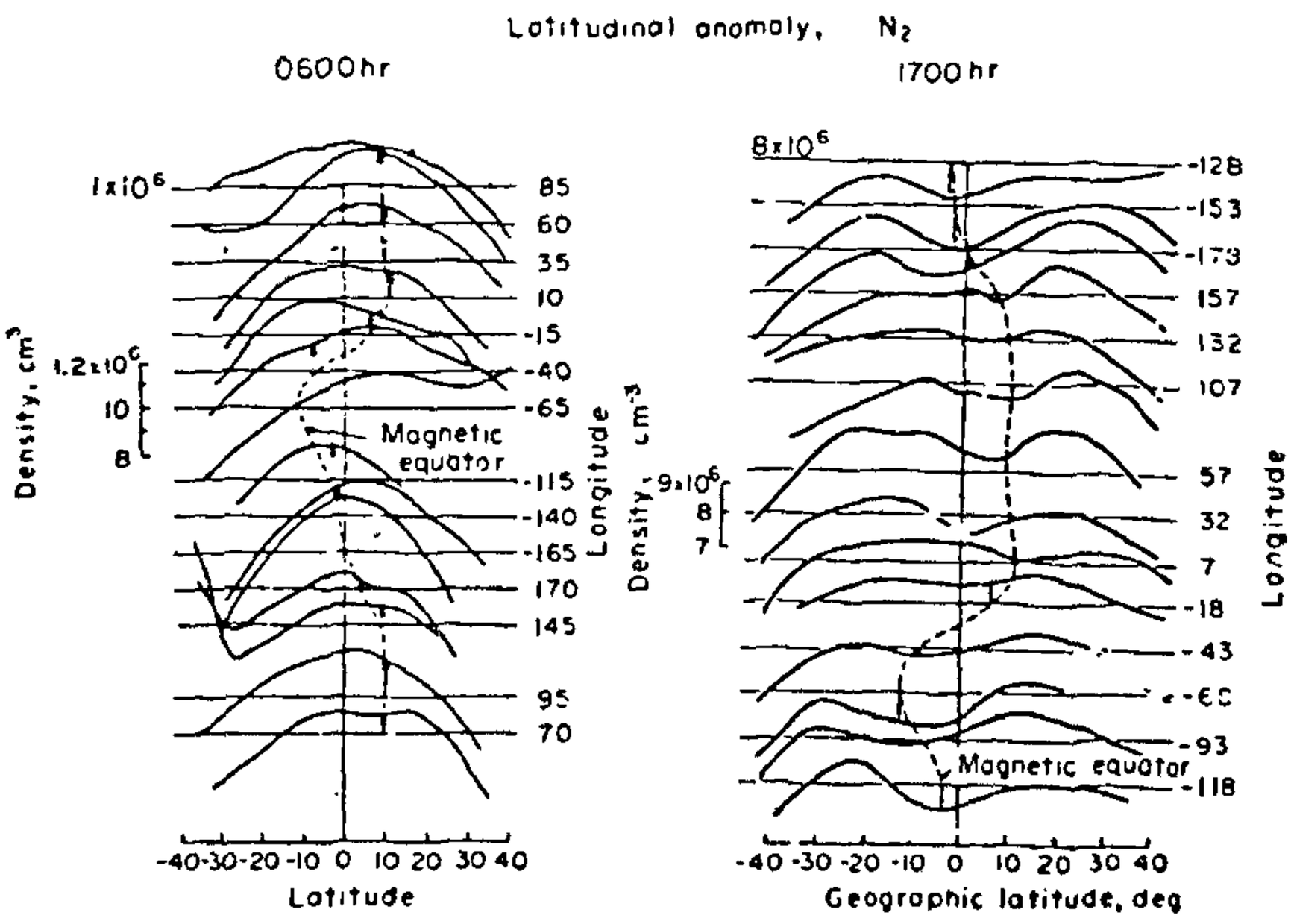

Figure 8. Latitudinal distribution of molecular nitrogen (N_2) in the morning and evening hours depicting the dip latitude dependence of the neutral composition similar to the *F*-region ionization. Results based on OGO VI satellite data[19].

first evidence came about from OGO VI data during high solar activity[19]. It was shown that N_2 and O densities also had their latitudinal distribution with crests (10–20%) on either side of the dip equator (± 20), similar to the charged particles during noon hours. Initially at dawn the neutral density maximum was located over the dip equator (Figure 8). Using a quasi 3-D model Hedin and Mayr[19] explained that at the latitude of the ionization crest ($\pm 20°$ dip lat.) the energy transport by the thermospheric circulation from the hot dayside to the cold nightside is damped by the increased ion drag. As a result there is a build-up of neutral density at these latitudes. Closer inspection of such an interaction process indicates that due to the enhanced ion drag the winds that redistribute the energy from the hot to the cold side get impeded and as a result more energy is retained on the dayside. As a consequence one would expect to see higher neutral temperatures at the latitudes where the EIA crest is located. Such effects are theoretically predicted by Anderson and Roble[20]. Recent results based on DE-2 satellite data by Raghavarao *et al.*[21] provided the first experimental evidence for such interactive coupling to be present (Figure 9). A decrease in the zonal winds and an increase in the neutral temperatures have been measured at the location of the crests of EIA in the data from the wind and temperature spectrometer (WATS) and Langmuir probe obtained simultaneously. This effect, yet another strong case for the thermosphere ionosphere coupling, is termed as ETWA (equatorial temperature and wind anomaly). These results are fairly new and more intensive studies are being carried out to bring out all the characteristic variabilities of ETWA. There are indications already for the neutral atmospheric circulation pattern to get altered due to the two pressure ridges getting formed along with the EIA crests (Raghavarao, Personal communciation 1992). Indications exist for a meridional circulation cell to get formed which manifest itself as an upward wind at the crest latitude and downward wind at the dip equator. The presence of such downward winds especially during evening twilight periods is likely to have significant control on the triggering of equatorial spread-*F* (ESF) (Figure 10) which is one of turbulent conditions of the equatorial *F* region[22]. ESF is formed due to plasma instability processes operating in the evening/night-time equatorial *F* region. However, apart from the electric field and the *E* region conductivities, the neutral dynamical parameters have been shown to be extremely important in the triggering of the instability[23,24].

Once triggered, the ESF manifests itself into a spectrum of irregularities with scale sizes ranging from millimeters to hundreds of kilometers. Fluctuating electric fields are also present. Since the ESF irregularities are magnetic field-aligned, the Joule heating effects associated with these fluctuating electric

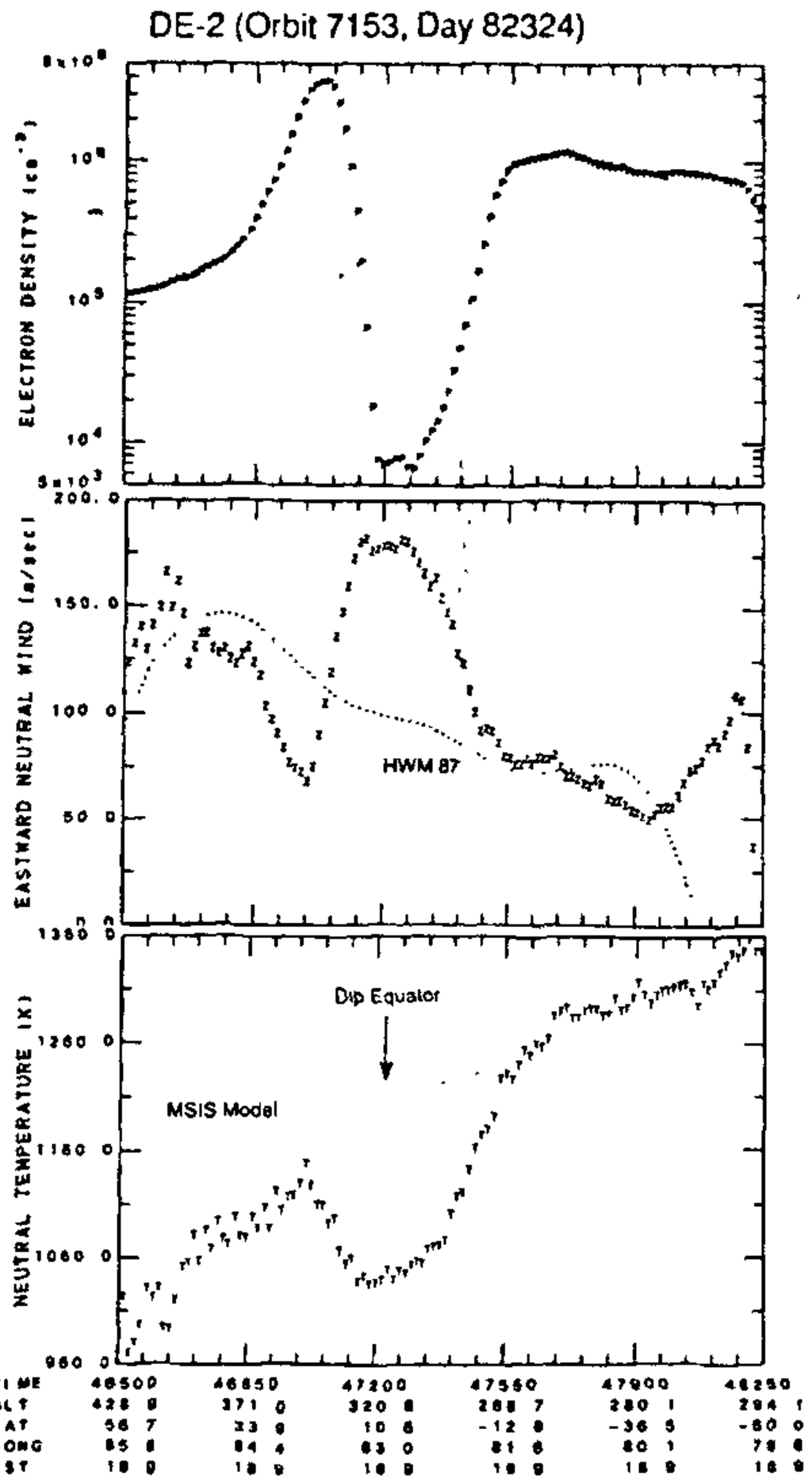

Figure 9. Development of ETWA in the equatorial latitudes based on simultaneous measurements of electron density, neutral temperature and neutral winds, once again demonstrating the close interaction of the neutral and ionized constituents of the upper atmosphere[21].

fields have been shown to be a significant source of heat input along the magnetic flux tubes and are capable of enhancing the neutral temperatures even by as large as 200–300 K[25]. It had been shown experimentally by Rajaraman *et al.*[26] that such enhanced temperatures are often seen over Mt. Abu and are well correlated with spread *F* occurrence over the equator (Figure 11). Once there is an enhancement in neutral temperature, it had already been shown that the *F*-layer height would have a corresponding change[17].

On the whole, ESF is controlled by the *E*-region conductivity, electric field as well as by neutral densities and neutral dynamics. It has the capacity to

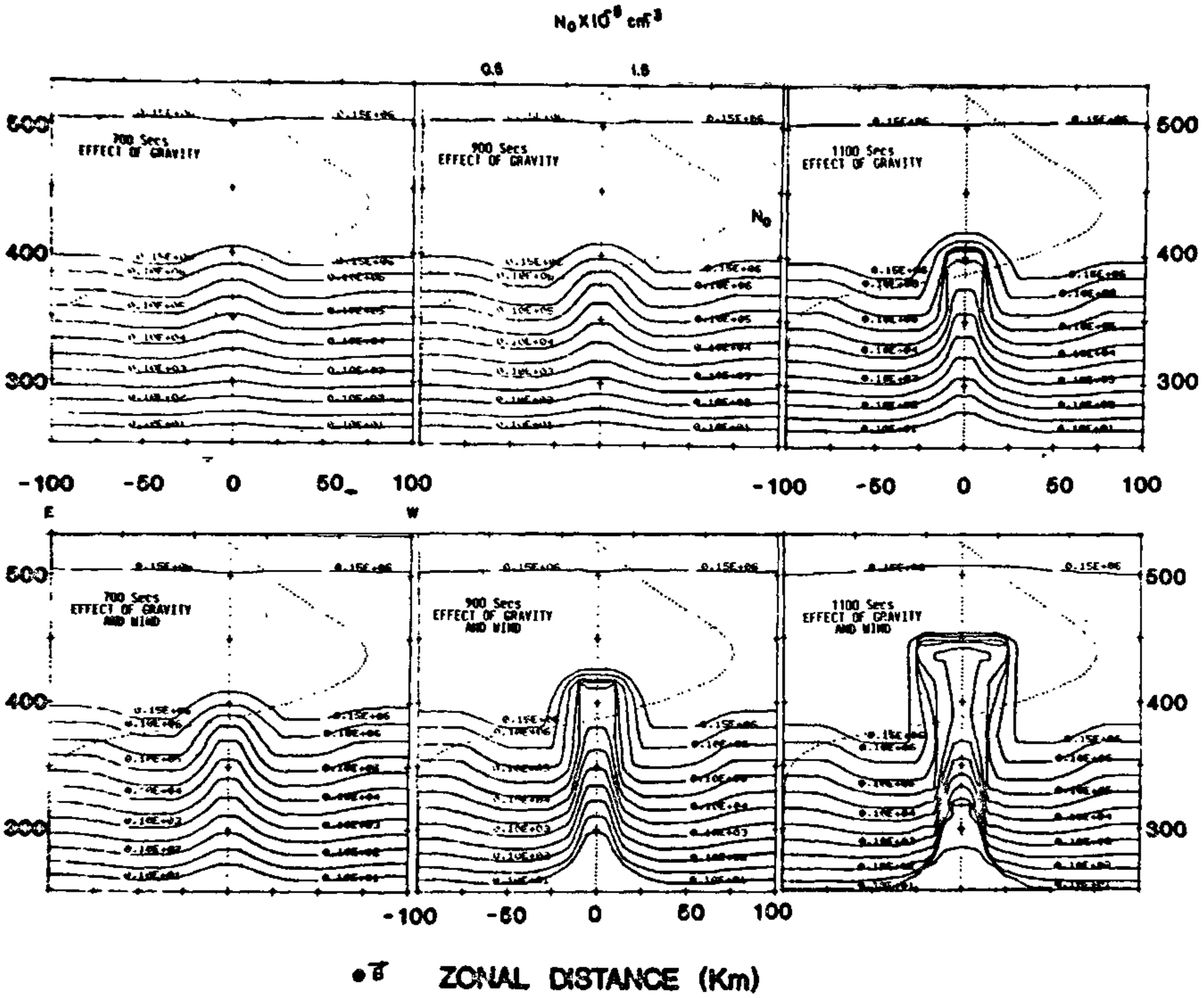

Figure 10. Results from a complex numerical simulation of the evolution of plasma depletions in the equatorial *F*-region demonstrating the significant role the vertical winds could play. The vertically downward winds have been shown to accelerate the evolution of a plasma depletion (bottom) for identical background conditions[22].

alter the neutral atmospheric parameters in a far away region, only to be linked by the magnetic field lines which in turn would alter the *F*-region heights. It is indeed a perfect example of a complex interactive thermosphere–ionosphere coupling process.

While discussing EIA and associated processes, one of the significant developments in recent years has been in the capabilities to retrieve faint emission features in the presence of bright background continuum. On account of this unique development in PRL, continuous measurements of daytime airglow emissions have become possible[27]. The investigation of processes related to thermosphere/ionosphere coupling by ground-based optical techniques that were until now restricted to only moonless periods of any night, could now be carried out even during broad daylight and clear sky conditions. The first results revealed that even during daytime conditions the *F*-region plasma densities have significant control on the thermospheric dayglow emission[28] (Figure 12). Coordinated ionospheric and dayglow measurements have revealed that the plasma densities are solely responsible for all the temporal variabilities exhibited by the same[29] (Figure 13). Large-scale features possibly associated with the development of EIA have been identified and interpreted using such measurements[29].

There are several other phenomena like the midnight temperature and pressure bulge over the dip equator which is believed to be formed due to the tidal mode coupling. The neutral wind diurnal variation is coupled to the ion density diurnal variation through the ion drag, thereby producing a semidiurnal term insitu[30] (Figure 14). In the study of this feature, both the propagating tides from the lower atmosphere to higher

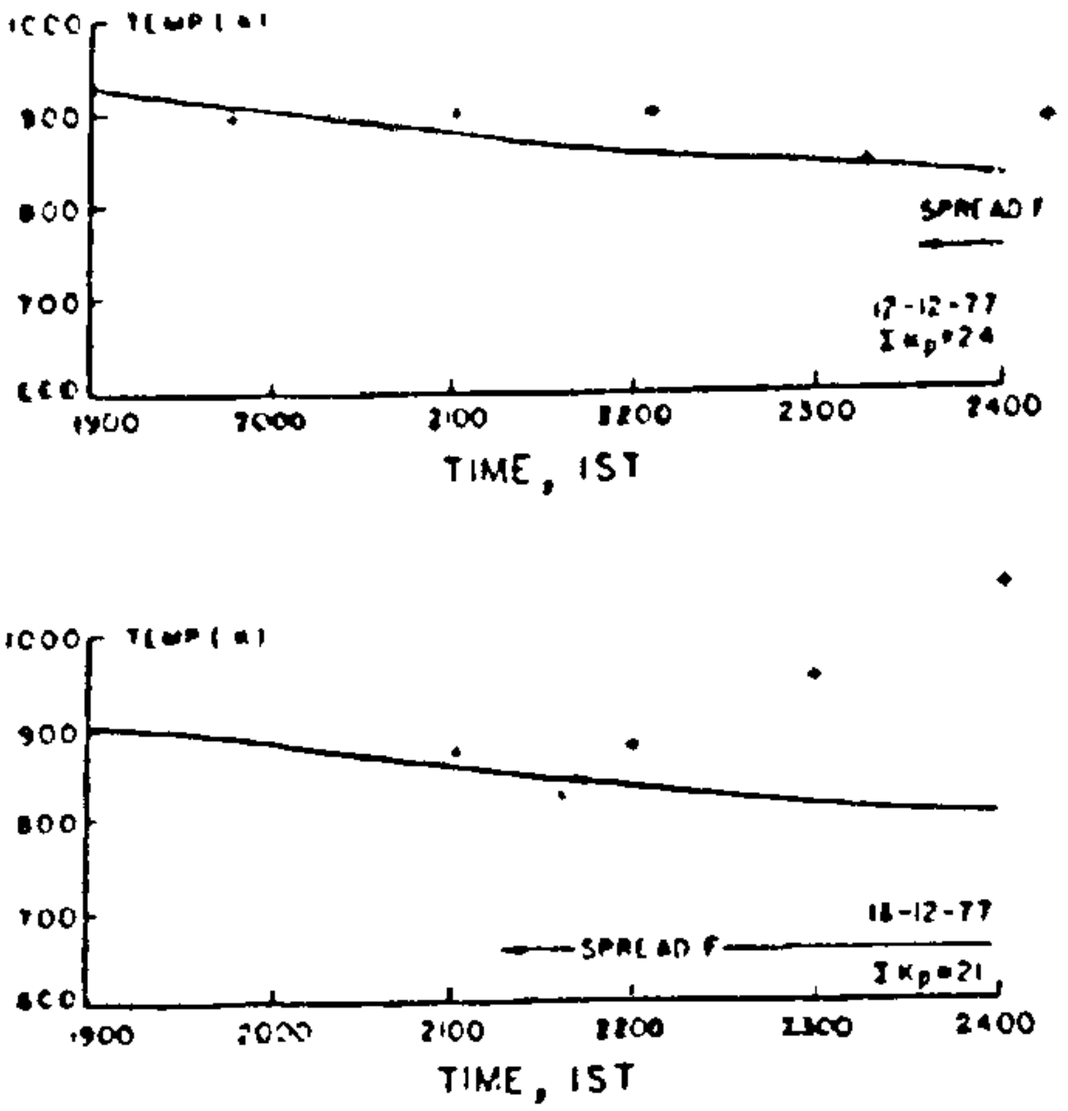

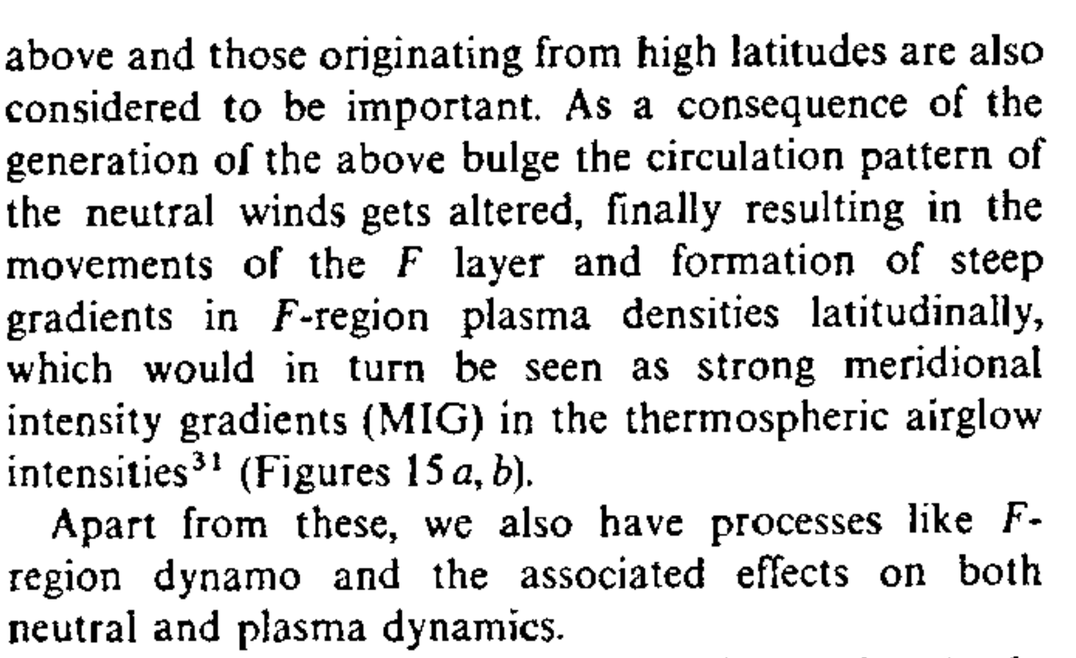

Figure 11. Experimental evidence for the enhanced neutral temperatures over latitudes away from the equator (Mt. Abu 20.4° N dip lat) to be possibly associated with spread-*F* over the dip equator, suggesting that the Joule heating due to the fluctuating electric fields associated with spread-*F* could possibly be the cause for the enhanced T_n[26].

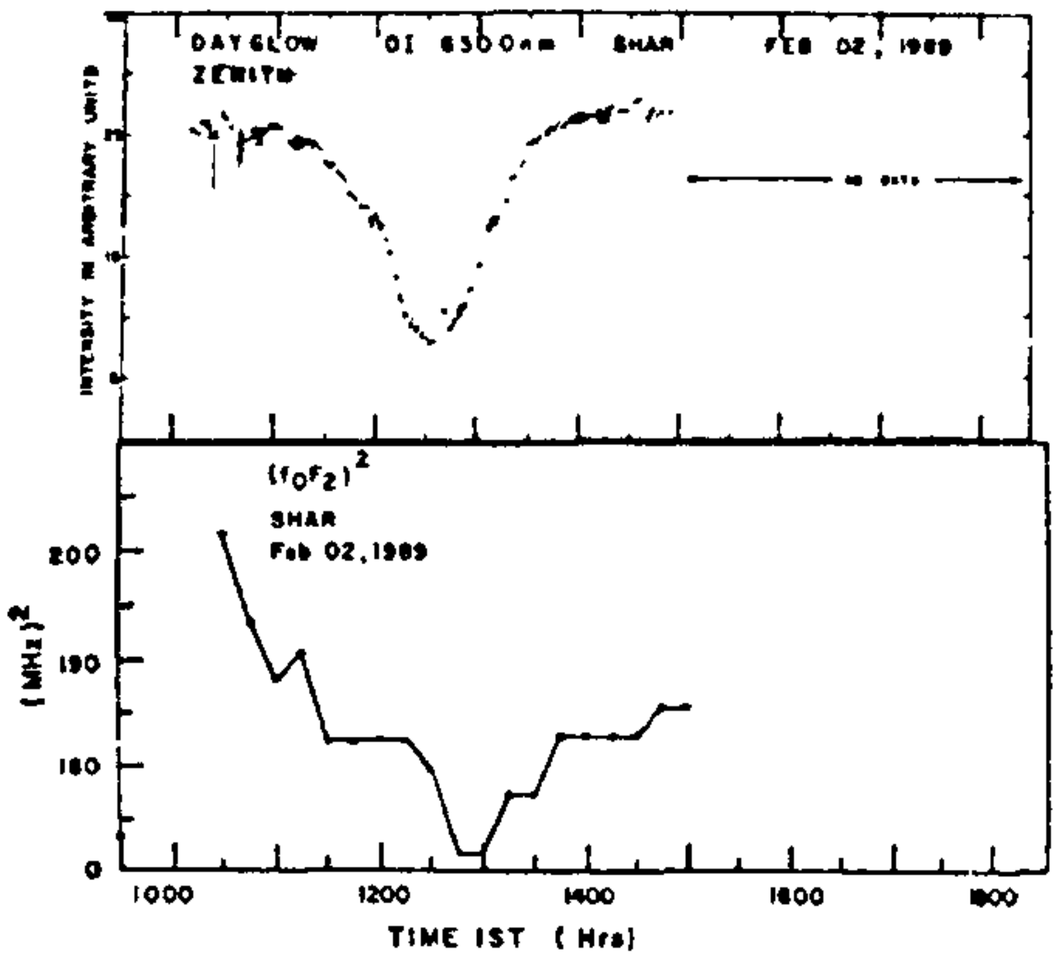

Figure 12. One of the first continuous measurements of OI 630.0 nm from SHAR (top) revealed the close coupling between the *F*-region plasma densities (bottom) and the 630.0 nm dayglow emission indicating the dissociative recombination to be significant even during daytime conditions[28].

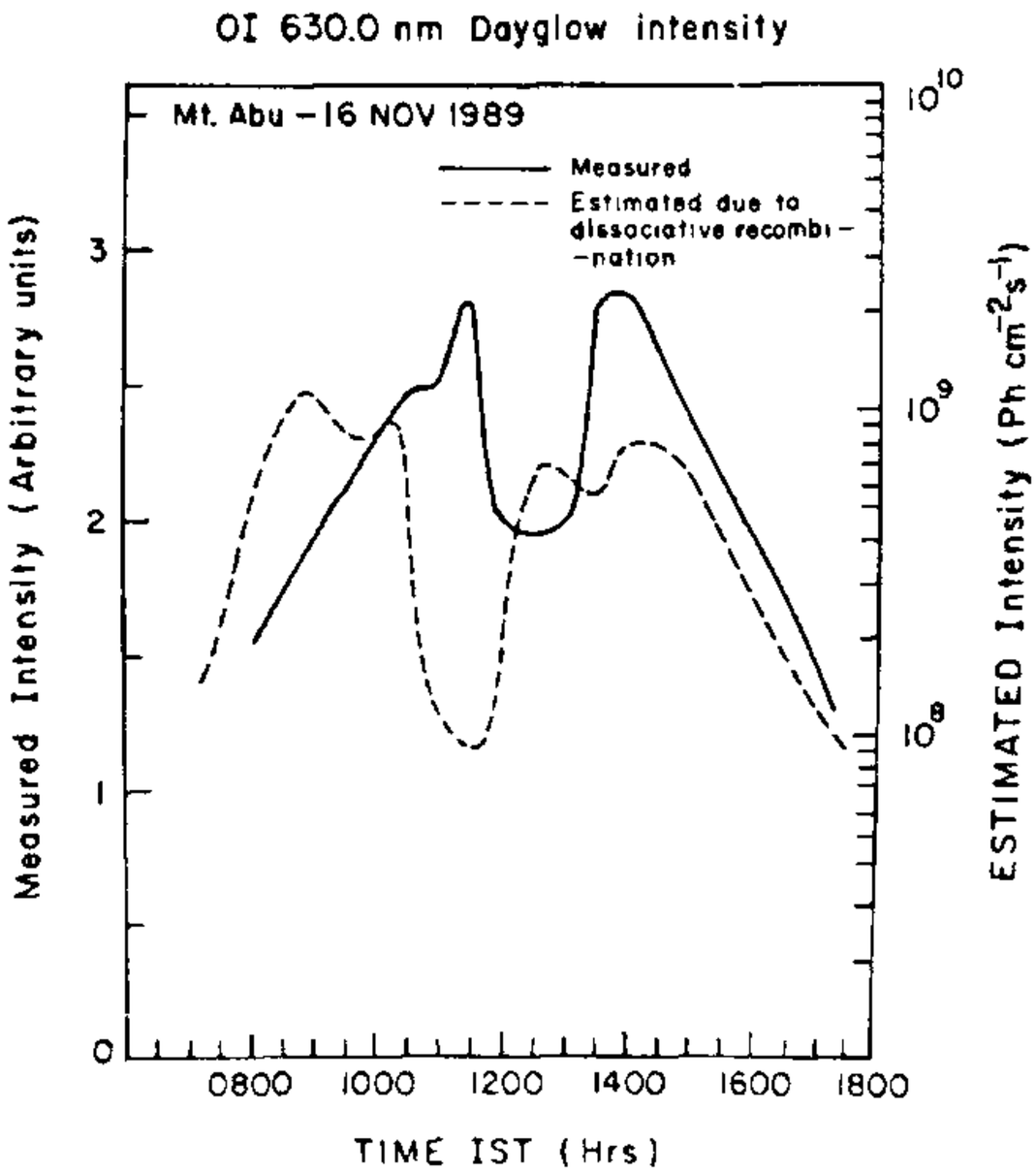

Figure 13. Measured and estimated intensities of OI 6300 nm dayglow for Mt. Abu and Ahmedabad. The estimated intensities are for the dissociative recombination in which the measured *F*-region electron densities (Ahmedabad) are used The time difference is ascribed to the physical separation (2° lat) of Mt. Abu and Ahmedabad and the evolution of the Equatorial Ionization Anomaly (EIA). Variation in the plasma densities is suggested to be solely responsible for the observed dayglow variations[29].

above and those originating from high latitudes are also considered to be important. As a consequence of the generation of the above bulge the circulation pattern of the neutral winds gets altered, finally resulting in the movements of the *F* layer and formation of steep gradients in *F*-region plasma densities latitudinally, which would in turn be seen as strong meridional intensity gradients (MIG) in the thermospheric airglow intensities[31] (Figures 15 *a*, *b*).

Apart from these, we also have processes like *F*-region dynamo and the associated effects on both neutral and plasma dynamics.

Most of the processes discussed so far, evolve slowly and have some sort of a systematic behaviour. Sudden impulsive inputs like what one encounters during a geomagnetic storm provide deeper insight into the coupling mechanisms and also about the relative

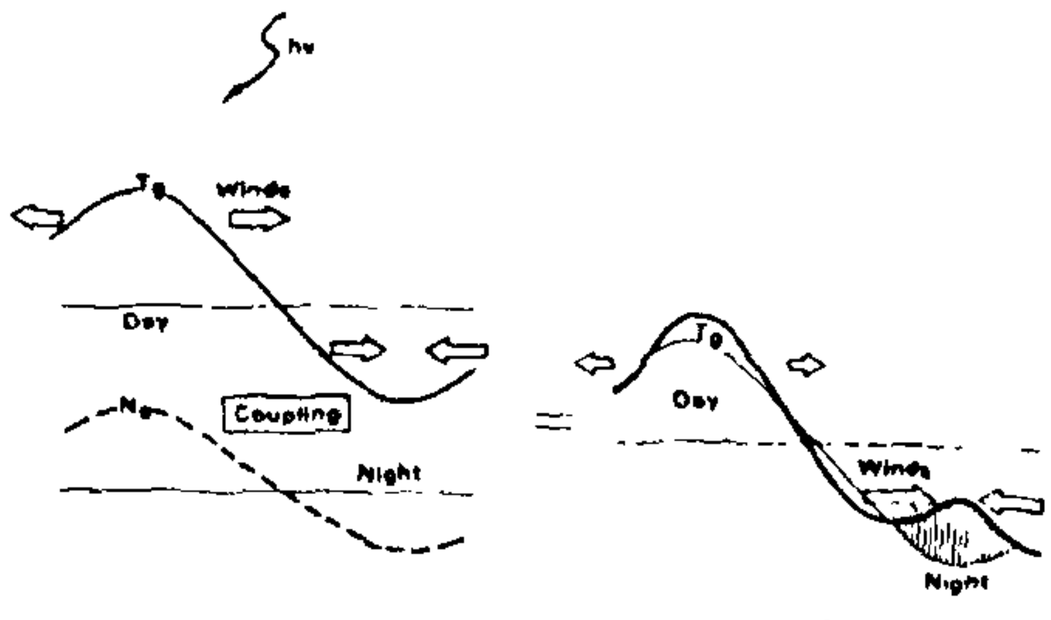

Figure 14. *Schematic representation of the interaction between the diurnal variation in ion drag and wind fields resulting in the midnight temperature bulge*[30].

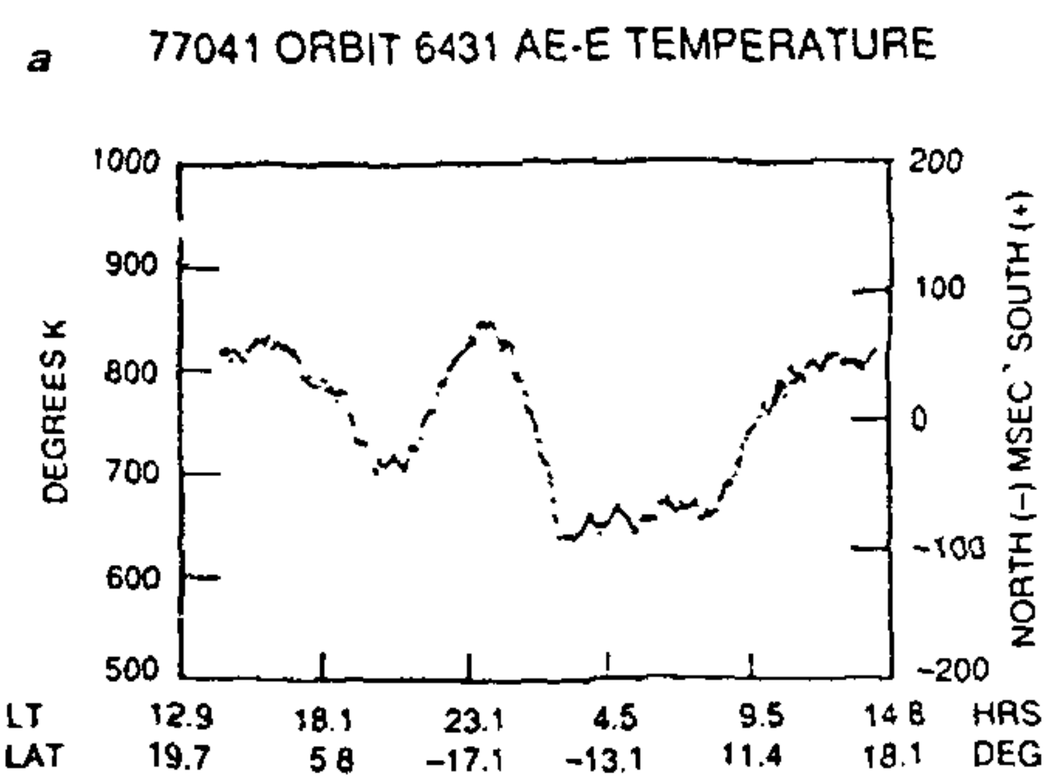

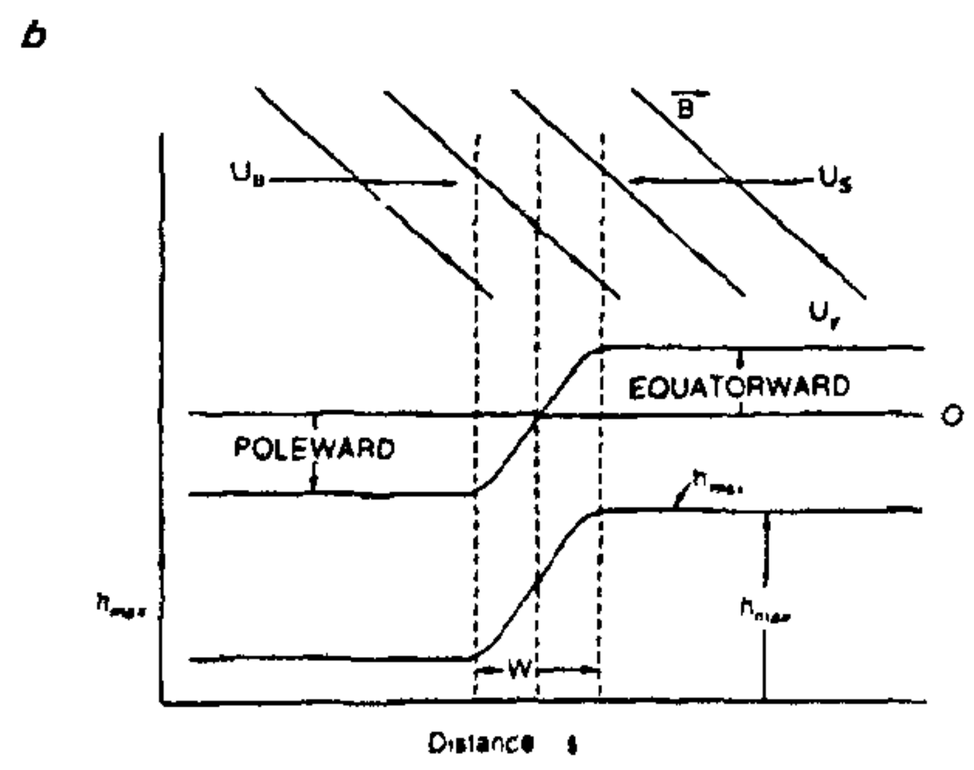

Figure 15. ***a***, Midnight temperature maximum over the equator as seen by the Atmospheric Explorer Satellite (AE-E) ***b***, Consequent midnight pressure bulge results in poleward winds pushing the *F*-layer down along the magnetic field lines. The already prevalent equatorward wind pushes the *F*-layer up. This would manifest as steep gradients in the *F*-region plasma density away from the equator and could be seen as Meridional Intensity Gradients (MIG) in 630.0 nm airglow intensity originating in the thermosphere[31].

importance of the various atmospheric/ionospheric parameters. Controlled theoretical simulation experiments are extremely useful in this regard wherein the effects of a typical parameterized geomagnetic storm could be simulated and compared with actual observations[12]. Complex interactive thermospheric/ionospheric general circulation models are being formulated taking into account all the known interactive processes with a primary aim of being able to predict the spatial and temporal morphology of the thermosphere/ionosphere system. Considerable progress has been made in recent years and still more is to come in the coming years.

1. Mayr, H. G., Harris, I. and Spencer, N. W., *Rev. Geophys. Space Phys.*, 1978, **4**, 539–565.
2. Jacchia, L. G., *Nature*, 1959, **183**, 1662–1663.
3. Taeusch, D. R., Carignan, G. R. and Reber, C. A., *J. Geophys. Res.*, 1971, **76**, 8318–8325.
4. Trinks, H., Fricke, K. H., Laux, U., Prolss, G. W. and Von Zahn, U., *J. Geophys. Res.*, 1975, **80**, 4571–4575.
5. Hays, P. B., Jone, R. A. and Rees, R. H., *Planet. Space Sci.*, 1973, **21**, 559–573.
6. Prolss, G. W., *J. Geophys. Res.*, 1981, **86**, 2385–2396.
7. Roemer, M., *Ann. Geophys.*, 1969, **25**, 419–437.
8. Prolss, G. W., Roemer, M., *Adv. Space Res.*, 1985, **5**, 193–202.
9. Mayr, H. G. and Volland, H., *J. Geophys. Res.*, 1972, **77**, 6774.
10. Ranjan Gupta, Desai, J. N., Raghavarao, R., Sekar, R., Sridharan, R. and Narayanan R., *Geophys. Res. Lett.*, 1986, **13**, 1055–1058.
11. Burrage, M. D., Abrew, V. J. and Orsini, N., *J. Geophys. Res.*, 1992, **97**, 4177–4187.
12. Rishbeth, H., *J. Atmos. Terr. Phys.*, 1979, **41**, 885–894.
13. Forbes, J. M. and Roble, R. G., *J. Geophys. Res.*, 1990, **95**, 201–208.
14. Rishbeth, H., *J. Atmos. Terr. Phys.*, 1967, **29**, 225–238.
15. Rishbeth, H., Ganguly, S. and Walker, J. C. G., *J. Atmos, Terr Phys.*, 1978, **40**, 767–784.
16. Miller, K. L., Torr, D. G. and Richards P. G., *J. Geophys. Res.*, 1986, **91**, 4531–4535.
17. Sridharan, R., Gurubaran, S., Raghavarao, R. and Suhasini, R., *J. Atmos. Terr. Phys.*, 1991, **53**, 515–519.
18. Gurubaran, S. and Sridharan, R., *J. Geophys. Res.*, 1992 (accepted for publication).
19. Hedin, A. E., and Mayr, H. G., *J. Geophys. Res.*, 1973, **78**, 1688–1691.
20. Anderson, D. N., and Roble, R. G., *J. Geophys. Res.*, 1974, **79**, 5231–5236.
21. Raghavarao, R., Whartson, L. E., Spencer, N. W., Mayr, H. G. and Brance, L. H., *Geophys. Res. Lett.*, 1991, **18**, 1193–1196.
22. Raghavarao, R., Sekar, R., and Suhasini R., *Adv. Space Res.*, 1992, **12**, 227–230.
23. Kelley, M. C., *J. Atmos. Terr. Phys.*, 1985, **47**, 745.
24. Raghavarao, R., Gupta, S. P., Sekar, R., Narayanan, R., Desai, J. N. and Sridharan, R., *J. Atmos. Terr. Phys.*, 1987, **49**, 485–492.
25. Cole, K. D., *J. Atmos. Terr. Phys.*, 1974, **36**, 1099–1102.
26. Rajaratnam, T. N., Desai, J. N., Degaonkar, S. S. and Cole, K. D., *Nature (London)*, 1978, **272**, 516.
27. Narayanan, R., Desai, J. N., Modi, N. K., Raghavarao, R., Sridharan, R., *Appl. Opt.*, 1989, **23**, 2138–2142.
28. Sridharan, R., Raghavarao, R., Gurubaran, S. and Narayanan, R., *J. Atmos. Terr. Phys.*, 1991, **53**, 521–528.
29. Sridharan, R., Haider, S. A., Gurubaran, S., Sekar, R., and Narayanan, R., *J. Geophys. Res.*, 1992, **97**, 13715–13721.

30. Mayr, H. G., Harris, I., Spencer, N. W., Hedin, A. E., Wharton, L. E., Porter, H. S., Walker, J. C. G. and Carlson, H. C., *Geophys. Res. Lett.*, 1979, **6**, 447–450.
31. Herraro, F. A., Spencer, N. W., Mayr, H. G., *Adv. Space. Res.*, 1992, **13**, 201–220.

ACKNOWLEDGEMENTS. Thanks are due to Prof. R. Raghavarao for making available some of his recent results on ETWA-related processes.

Received 22 December 1992; accepted 6 January 1993

RESEARCH COMMUNICATIONS

Endomyocardial fibrosis is possibly an interstitial heart disease

C. C. Kartha

Division of Pathology, Sree Chitra Tirunal Institute for Medical Sciences and Technology, Thiruvananthapuram 695 011, India

To obtain clues to the pathogenesis of endomyocardial fibrosis (EMF), autopsy material from 42 patients and biopsy specimens from 89 patients were studied histologically. When full blown EMF was present in one cardiac ventricle, the contralateral ventricle with either focal lesions or no visible lesions, had interstitial fibrosis associated with increase in interstitial cellularity. It is suggested that EMF may be a reactive and progressive interstitial fibrosis, a result of cardiac fibroblast growth, with or without proliferation and enhanced collagen synthesis.

SINCE Gopi's[1] discovery of the prevalence of endomyocardial fibrosis (EMF) in Kerala, the disease has been extensively characterized in terms of clinical, radiological and echocardiographic features[2]. The pathological profile of the disease in Kerala has also been described in detail[3,4]. However, the pathogenesis of the disease remains unclear and the early lesion elusive. In the study reported here, pathological material has been analysed to obtain evidence of early or active lesions and identify histological features which would provide clues to the pathogenetic mechanisms.

Autopsy material from 42 patients who died of EMF and biopsy specimens from 89 patients with EMF, who underwent endocardiectomy and valve replacement from 1981 to 1991, form the basis of this study. The hearts at autopsy were examined in detail for gross lesions of the endocardium, myocardium, valves and coronary arteries. Paraffin sections from tissue blocks, representing all chambers of the heart, including the uninvolved portions, stained with haematoxylin and eosin were available from autopsy material. Biopsy material from operated patients also included right ventricular specimens from 27 patients with left ventricular disease.

In the absence of a gold-standard for early or active EMF, early disease was suspected in young patients, and in contralateral ventricles with either visible focal lesions or absence of visible lesions, when extensive disease was present in one ventricle. Patients were divided into two groups, viz. those up to the age of 13 years and those above the age of 13 years.

Histologic criteria evaluated were: (1) nature of collagen, (fibrillar or hyalinized), cellularity, inflammation and calcification in the endocardium, (2) degenerative or hypertrophic changes in the myocardium, (3) cellularity (inflammatory or fibroblastic) and fibrosis (pericellular, perivascular, plexiform or scars) in the interstitium, and (4) vascular lesions (arteritis, mural thickening).

The plan was to observe whether in 'suspected early EMF' pathogenetic clues, viz. myocyte necrosis, inflammatory lesions, small vessel disease or endocardial thrombosis, were present.

The details of specimens reviewed in the study, classified in terms of ventricular involvement of the disease as well as age and sex of the patients, are given in Tables 1 and 2. Histologic features in autopsy specimens, depending on the age of patients, are summarized in Table 3. No significant difference was observed between the two age groups. Also, when extensive disease was present in one ventricle, the contralateral ventricle with either mild or no visible

Table 1. Details of autopsy specimens ($N = 42$)

	Age 0–13 years		Age > 13 years	
	Male	Female	Male	Female
BV EMF	1	1	0	1
With valve disease	0	0	3	1
LV EMF				
No RV lesion	0	0	2	1
Focal RV lesion	1	1	3	6
With TOF	0	0	1	0
RV EMF				
No LV lesion	5	0	6	3
Focal LV lesion	0	0	0	1
With valve disease	1	0	2	2

BV, Biventricular; EMF, endomyocardial fibrosis; LV, left ventricle; RV, right ventricle; TOF, tetralogy of Fallot.